MHD Stability at the Edge Region in H-mode Plasmas with Long Edge-Localized-Mode (ELM) Free Phases in LHD

K. Toi, S. Ohdachi, R. Ueda, K.Y. Watanabe, T. Nicolas, Y. Suzuki,
K. Ogawa, K. Tanaka, Y. Takemura and LHD Experiment Group

National Institute for Fusion Science, Toki 509-5292, Japan

Abstract

Clear suppression of magnetic fluctuations associated with resistive interchange modes (RICs) is observed during long ELM (edge localized mode)-free phases of the H-mode plasma in an outward-shifted configuration of LHD, in which plasma a steep pressure gradient is generated at the plasma edge in the magnetic hill. The ELM free H-phase is interrupted by large amplitude ELMs which are thought to be induced through nonlinear evolution of the RICs having m=1/n=1 dominant component (m: poloidal mode number, n: toroidal one). The m=1/n=1 RIC amplitude is enhanced about 10 times compared with the H-phase level during each ELM. In most of the H-mode shots, the final ELM free phase returns to L-phase by a large amplitude ELM. In the L-phase the RIC amplitude is enhanced by a factor of ~ 3 compared with that in the H-phase, although the edge pressure gradient is reduced considerably. Linear resistive MHD stability analysis is attempted using experimentally obtained equilibrium profiles. From the numerical analysis, the distance between the location of the steepest pressure gradient and the main mode resonance surface, i.e., the rotational transform ι=1, is found to be important for the growth of the m=1/n=1 RIC in the H-mode plasma.

1. Introduction

MHD stability of H-mode plasmas with a steep pressure gradient in the edge region is crucially important for burning plasmas based on tokamak and stellarator/helical concepts. Once MHD instabilities are excited in the edge transport barrier (ETB) or pedestal region, strong degradation of plasma performance occurs. As commonly observed in major toroidal confinement devices, such MHD instabilities often trigger large amplitude edge localized modes (ELMs) which affect seriously the life of divertor target plates and other plasma facing components [1, 2]. In tokamak plasmas, the MHD instabilities triggering the so-called type I ELMs through the nonlinear evolution are thought to be ballooning and/or peeling modes and their

combinations [3,4]. The instabilities are driven by pressure gradient and toroidal current density at the ETB or pedestal region. On the other hand, ELMs are also observed in H-mode plasmas of stellarator/helical devices. In contrast to tokamak H-modes, pressure driven modes such as resistive interchange modes are thought to be the likely candidates of an ELM trigger through the nonlinear evolution, as discussed in W7-AS and LHD H-mode plasmas [5-8]. In LHD, the soft X-ray fluctuations associated with the MHD instabilities in the edge of the H-mode plasmas show the non-ballooning character in clear contrast to the tokamak H-mode. The MHD instabilities were concluded to be resistive interchange modes (RICs), since the edge region of the H-mode is stable for ideal interchange modes and ballooning modes [9]. In this paper, we present experimental results on clear suppression and large growth of RICs in H-mode plasmas having long duration of ELM free phases achieved in an outward-shifted magnetic configuration of R_{ax}=3.9m in LHD, where R_{ax} is the magnetic axis position in the vacuum field. We attempt qualitative interpretations of these experimental observations with the assistance of a linear resistive MHD stability analysis.

This paper is organized as follows. In Section 2, the characters of the H-mode in the outward-shifted configuration are presented, being focused on edge MHD stability. Rapid and large growth of RICs and excitation of large amplitude ELMs observed in the H-modes are described in Section 3. In Section 4, linear resistive MHD stability analysis is attempted for the equilibrium pressure profiles obtained in H- and L-phases. In Section 5 some important issues in experimental observations and the numerical analysis on RICs are discussed. The main results are summarized in Section 6.

2. Suppression of RICs in ELM free phases of the H-mode

In LHD, an H-mode plasma was first obtained in the so-called inward-shifted magnetic configuration of R_{ax}=3.6 m [6, 7]. Although better particle confinement is expected in the configuration compared with the outward-shifted configuration of R_{ax} = 3.9 m, the MHD stability is worse due to the presence of high magnetic hill in the edge region and RICs are easily destabilized, in particular, in the ETB region of H-mode plasmas. In the inward-shifted configuration, the most dangerous RIC is the m=2/n=3 mode where m and n are the poloidal and toroidal mode numbers, respectively. The m=2/n=3 RIC is always destabilized just after the ETB formation by the L-H transition where the low order resonant surface ι=3/2 resides in the ETB region. Ideal interchange modes are stable in the ETB region of the H-modes so that RICs play an

important role in edge MHD stability of the H-mode plasmas in LHD. It is known that RIC usually has a character of the mode localized at the mode resonance surface, and has an even function around the resonance surface. If the locations of the low order resonant surfaces are controlled in order to be placed distant from the steep pressure gradient region, RIC activities would be considerably reduced to an acceptable level for good plasma confinement. However, so far this scenario was not achieved in H-mode plasmas obtained in the R_{ax}=3.6m configuration.

In a specific outward-shifted configuration, i.e., the R_{ax}=3.9m configuration of LHD the main low order resonance surface ι=1 is placed just outside the last closed flux surface (LCFS) defined in the vacuum field. In this configuration, the H-modes are routinely obtained in hydrogen target plasmas by moderate neutral beam injection (NBI) power of ~ 5MW at the toroidal field strength B_t~ 1T. The H-mode exhibits clearly different characters from those of the H-mode in the inward-shifted configurations. That is, the H-mode has ELM free phases of which durations are much longer than the global energy confinement time [8]. Two important features on edge MHD stability of the H-mode in the outward-shifted configuration are the appearance of long ELM-free phases and the interruption of the phases by large amplitude ELMs. A typical discharge waveform of the H-mode is shown in Fig.1(a). In Fig.1(b) time evolution of the root-mean-square amplitude of magnetic fluctuations with the m=1/n=1 structure is shown together with the volume averaged toroidal beta value measured by a diamagnetic loop $<\beta_{dia}>$. Note that higher harmonic fluctuations such as m=2/n=2, m=3/n=3 and others are also simultaneously destabilized during the ELM. In this shot, we pay attention to typical time slices in the characteristic confinement phases marked with “H” at t=4.533 s (H-phase) and “L” at t=4.700 s (L-phase). The radial profiles of electron density n_e, electron temperature T_e and the electron pressure P_e in these time slices are compared in Fig.2. As seen from Fig.2, an obvious ETB or pedestal having very steep gradient is formed in the n_e-profile at t=4.533 s in the ELM-free H-phase, but is not formed in T_e-profile. Nevertheless, the P_e-profile has also a clear ETB structure. In the L phase, no ETB structure is formed in both T_e- and n_e-profiles, and, accordingly, also not in the P_e-profile. Note that the vertical arrows in Fig.2 indicate the inferred locations of the ι=1 mode resonance surface. As seen from the P_e-profile in Fig.2, appreciable Shafranov shift is observed in both phases. Just before the H-L back transition at t=4.670 s, the magnetic fluctuation amplitude is in a very low level. Just after the back transition triggered by a large ELM the L-phase appears enhancing the magnetic fluctuation amplitude by a factor of ~3, compared with that in the H-phase. In contrast to the H-modes in the R_{ax}=3.9m configuration, no RIC suppression is

observed in H-modes in the inward-shifted configuration of R_{ax}=3.6m.

3. Large growth of RICs at the onset of a large ELM

As seen from Fig.1, long ELM free phases are interrupted by large amplitude ELMs. It is interesting to clarify the main triggering mechanism of large ELMs in the H-modes in LHD. The averaged diamagnetic beta $<\beta_{dia}>$ at the onset of each ELM is not always the same value and has a noticeable variation of ~ $\pm$6 % in the shot shown in Fig.1. This fact suggests that the important driving factor of RIC is the pressure gradient at the relevant mode resonance surface (in this case ι=1) rather than the global value $<\beta_{dia}>$ in the H-mode plasma. In the vacuum magnetic configuration of R_{ax}=3.9 m, the ι=1 surface locates at the normalized minor radius $<r_s>/<a>=\rho_s$=1.02, that is, just outside the last closed magnetic surface (LCFS) in the vacuum configuration. The MHD equilibrium of a finite beta plasma was calculated by the HINT-2 code where the existence of the nested magnetic surfaces is not assumed a priori [10]. It is inferred from the ι-profile calculated by the HINT-2 code that the ι=1 surface locates at the normalized minor radius $<r_s>/a=\rho_s$ ~1.08 (a: averaged minor radius) just outside the LCFS defined by the boundary of the nested magnetic surface region in the finite beta H-mode plasma. Of course, the ι=1 surface may be determined experimentally, for instance, by soft X-ray (SX-) fluctuation signals due to the m=1/n=1 mode in the H-mode. However, the SX-fluctuations are too weak to determine the ι=1 location, because the resonance surface location is in very low T_e region. Instead, an array of H_α emission detectors with high time response clearly detected the H_α fluctuations of the m=1/n=1 mode in the L-phase because of relatively high neutral density outside the LCFS [11]. Figure 3 shows the profile of the H_α fluctuation amplitude associated with the m=1/n=1 mode (δI_α: open triangles) and the coherence with magnetic probe signals ($\gamma_{H\alpha\text{-}MP}$: open circles) as a function of the normalized vertical coordinate Z/Z_a in the horizontally elongated section of the plasma, where Z_a defines the LCFS in the vertical direction. The peaks of these quantities are found at $Z/Z_a \sim \rho_s \sim 1.05$ just outside the LCFS. The correlation analysis is applied to the time window from t=4.70s to 4.75s including the L-phase. The observed frequency of the m=1/n=1 mode propagating in the electron diamagnetic drift direction (f_{obs}) is ~4.5 kHz, of which frequency is determined by the sum of the mode frequency in the plasma frame f_{real} and the Doppler frequency due to ExB plasma flows f_{dop}. The frequency f_{real} of the low n RICs was confirmed to be nearly equal to the electron diamagnetic drift frequency f_{*e} in various plasma conditions of LHD [12]. The frequency f_{*e} evaluated at the inferred ι=1 surface is estimated to be ~ 0.4 kHz for the L-phase equilibrium profile. It

will become small further if the local flattening of the electron pressure profile at the ι=1 surface occurs due to the growth of RICs. Accordingly, the observed mode frequency (f_{obs}~4.5 kHz) is thought to be dominantly determined by the Doppler frequency corresponding to the ExB plasma flow in the electron diamagnetic drift direction. This means that the negative radial electric field E_r of ~10 kV/m is inferred at the ι=1 surface even in the L-phase. However, the experimental data of the E_r around the resonance surface are not available in the L-phase because electron temperature in the edge region is too low to obtain sufficient spectral emissions for charge exchange recombination spectroscopy.

A quiescent H-phase RICs are strongly suppressed is interrupted by a large amplitude ELM, as seen from Fig. 1. To clarify strong interaction between the m=1/n=1 RIC and the ELM, two ELM events are expanded in time in Fig.4, showing the temporal behaviors of poloidal magnetic fluctuation signal (b_θ) together with the edge line-electron-density (n_eL_{edge}) and the H_α emission signal. As seen from the figure, the weak m=1/n=1 mode fluctuations b_θ in the ELM free phase begin to grow rapidly about 1ms before the onset of an ELM of which signature is the small crash in n_eL_{edge}. The H_α emission rises rapidly ~0.1 ms after the small n_eL_{edge} crash. The rapid growth of the m=1/n=1 RIC induces an ELM event, and in turn ELM enhances the RIC further. The magnetic fluctuation amplitude during the ELM is enhanced by a factor of ~10 higher than the ELM-free H-phase level and ~3 times higher than the L-phase level. It should be noted that magnetic fluctuations b_θ of the m=1/n=1 RIC growing rapidly just prior to the ELM could trigger the ELM, at even low amplitude of b_θ. Immediately after the small crash, strong and complex coupling between RIC and ELM takes place and leads to further increasing the RIC amplitude and full development of an ELM crash. Finally, the coupled ELM and RIC reduces the pressure gradient around the ι=1 surface substantially, and then the RIC together with ELM is suppressed as in the previous ELM free phase. In addition to the above-mentioned dynamic behaviors of the ELM event, it should be noted that the mode frequency f_{obs} is fairly low (~0.5 kHz) in the ELM free H-phase and then increases noticeably during the ELM, as seen from Fig.4. Although the b_θ waveform is considerably deformed during the ELM, the frequency of the dominant m=1/n=1 component is f_{obs}~ 2-3 kHz. Since the mode frequency in the plasma frame estimated with f_{*e} is ~ 3 kHz in the H-phase and ~0.4 kHz during the ELM using the equilibrium pressure and density profiles in the H-phase and the L-phase in which the profiles are nearly same as those during the ELM [8], the frequency f_{obs} is dominantly determined by the Doppler frequency f_{dop} due to the ExB plasma flow. The frequency f_{dop} is

thought to be determined by the flow in the ion diamagnetic drift direction in the H-phase and by the flow in the electron diamagnetic drift direction during the ELM. However, the experimental data of E_r are not available at the ι=1 surface both in the H-phase and during ELM.

Focused on the time derivative of the stored energy derived from a diamagnetic loop dW_p/dt just before each ELM in the H-mode, it increases appreciably with positive sign from about 30 ms prior to the ELM event, which suggests a small increase in W_p. Since T_e- and n_e-profiles are measured every 20 ms to 33 ms by Thomson scattering in the H-mode shots, it is difficult to capture the profile changes about 1 ms prior to an ELM event. In the H-mode shot, the profiles are occasionally obtained 6 ms prior to a large ELM. The comparison of the profiles with those measured 23 ms prior to the ELM shows that the edge pressure gradient is maintained nearly the same until 6 ms prior to the ELM, while the W_p increases slightly. From the observations, the slow increase in W_p under the condition of unchanged pressure gradient in the edge suggests a small expansion of the radius of the steepest pressure gradient layer in the ETB. The expansion leads to a sudden increase in the pressure gradient at the ι=1 surface in the high magnetic hill region, so that the rapid growth rate of RICs may be inferred. However, it is a big challenge to confirm this possibility experimentally by monitoring the time evolution of the pressure gradient at the ι=1 surface with the available plasma diagnostics in LHD. Instead of the direct measurements, in the next Section 4, we investigate the possibility using linear stability analysis of m=1/n=1 RIC for the equilibrium data of the H-mode shown in Fig.2.

4. Stability analysis with a linear resistive MHD stability theory

In this section, the stability of RICs is analyzed for the equilibrium pressure profiles obtained experimentally, using a linear resistive MHD stability code which is applicable to a cylindrical plasma on a fixed boundary condition [13]. As the first step, the pressure profiles of the H-mode plasma are reconstructed using the normalized minor radius $x=<r>/a$, instead of the major radius R as in Fig.2. The pressure profiles $P_{eq}(x)$ in the H- and L-phases are fitted with the following analytic form:

$$P_{eq}(x)=\frac{1}{2}P_{ETB}[1-\tanh(\alpha(x-x_o))]+(P_o-P_{ETB})[1-x^{g0}]^{g1} \quad (1),$$

where $P_{ETB,}$ P_o, α, x_o, g_0 and g_1 are positive constants. The first term in the right-hand side of eq.(1) mainly determine the shape of the pressure profile in the plasma edge

region. The second term is used to reconstruct the pressure profile in the core region. The parameters P_{ETB} and P_o are the ETB or pedestal height of the pressure and the pressure on the magnetic axis, respectively. The parameter α characterizes the steepness of the pressure gradient in the ETB or pedestal, and x_o determines the radial location of the steepest pressure gradient layer. The scale length of the pressure gradient normalized by the minor radius L_p/a is expressed as $L_p/a \cong 1/(2\alpha)$ at $x=x_o$. For large α ($\gg$1), eq.(1) expresses the pressure profile with the ETB or pedestal very well. For small α in the order of unity, eq.(1) can also express the profile without the ETB or pedestal, as in the L-phase. The data points and the fitted curve of the pressure profiles in H- and L-phases with eq.(1) are shown in Fig.5, where the averaged minor radius a is adopted as a=0.466 m. The best-fitted curve in Fig.5 is expressed with eq.(1) having a parameter set of P_{ETB}=3.2 kJ/m^3, P_o=5.3 kJ/m^3, α=17.5, x_o=0.88, g_0=2.0 and g_1=3.5 for the H-phase, and a set of P_{ETB}=4.0 kJ/m^3, P_o=5.3 kJ/m^3, α=3.0, x_o=0.62, g_0=2.0 and g_1=12.0 for the L-phase. Here, the ι=1 surface location is inferred to be at $x_s=<r>/a \sim 1.05$ to 1.08 as discussed in Section 3.

The present version of the resistive MHD stability code is not straightforwardly applied to the equilibrium profiles shown in Fig.5. To overcome this difficulty, the averaged minor plasma radius a is expanded to include the ι=1 surface inside the LCFS as $x_s < 1$, instead of the situation such as $x_s \sim 1.05$. For the following stability analysis, the ι=1 location is placed at x_s =0.945 based on the rotational transform profile calculated by the HINT-2 code, when the averaged minor radius a is expanded to a=0.52 m by a factor of ζ=1.05/0.945=1.11. Using the normalized radial coordinates with the expanded a, the position of the steepest pressure gradient layer x_o corresponds to x_o=0.788 for the H-phase profile shown in Fig.5 and x_o=0.560 in the L-phase profile, respectively.

The linear stability analysis code is applied to the profiles obtained in the H-mode, because the analysis may be helpful for qualitative understanding of the MHD mode stability. The distance $|x_o - x_s|$ between the ι=1 location x_s and the steepest pressure gradient location x_o is a key parameter for the stability of m=1/n=1 RIC. In the ETB and the ι=1 resonance surface regions of the H-mode, the magnetic Reynold number S is in the range of 10^5 to 10^6. In the stability analysis, we employ the toroidal beta $\beta_{eq}(x)$ profiles derived from the $P_{eq}(x)$ profiles scanning the x_o-value, where B_t=0.9 T. The distance $|x_o - x_s|$ is scanned by increasing x_o from x_o=0.788, where the profile with x_o=0.788 is constructed from the H-phase profile obtained in the experiment (Fig.5(a)). It should be noted that the location of the ι=1 mode resonance surface is fixed as x_s=0.945 throughout the x_o scan. In the L-phase, x_o is scanned in the narrow

range from x_o=0.540 to 0.62, since the $\beta_{eq}(x)$ profile does not have an ETB structure. The profile with x_o=0.560 is constructed from the experimental profile shown in Fig.5(b). The increase in x_o simulates the radial expansion of the steepest pressure gradient layer in the ETB, and pushes the gradient layer to the ι=1 surface. The largest growth rates γ_1 calculated by the linear resistive code [13] are plotted as a function of x_o for both H and L-phases, in Fig.6(a) with linear-scale and in Fig.6(b) with log scale. Here, γ_1 is normalized with $\varepsilon V_A/a$ ($\varepsilon=a/R$, V_A is Alfvén speed, and a and R are respectively the averaged minor and major radii of the plasma) and the value of S=10^5 and 10^6 are adopted. For the H-phase, the growth rates are also calculated for much higher S value, i.e., S=10^8. In the H-mode plasma discussed in this paper, the normalization factor $\varepsilon V_A/a$ is in the range of ~1x10^6 (1/s) near the edge region. In the H-phase the growth rates increase quickly with decrease of the distance $|x_o$-$x_s|$, while the values in the L-phase show a weak dependence on x_o.

In Fig.7(a), the radial profile of $\beta_{eq}(x)$ with x_o=0.788 corresponding to the ELM free phase is shown as a function of the normalized minor radius x, together with the $\iota(x)$ profile. The m=1/n=1 mode eigenfunctions of the scalar potential ϕ_1 and pressure perturbation p_1 are shown in Figs.7(b), where S=10^5. The eigenfunctions of the poloidal flux ψ_1 and the radial displacement ξ_r are shown in Fig.7 (c). The radial displacement ξ_r is evaluated as $\xi_r = -\frac{m}{\gamma_1}\frac{\phi_1}{x}$. Although the gradient of $\beta_{eq}(x)$ is very small at the ι=1 surface in this profile, the largest growth rate γ_1 does not vanish as 1.546E-3 for S=10^5 as seen from Fig.6. The eigenfunction ϕ_1 has a strongly localized character even for low mode number m=1 and n=1, exhibiting a typical interchange mode feature. It should be noted that the peak of ϕ_1 is x=0.941 and is slightly shifted toward the steep pressure gradient region inward the ι=1 mode resonance surface. The small tail of ϕ_1 extends into the steep pressure gradient region, while ϕ_1 has a large peak at the mode resonance surface. The eigenfunction p_1 has a double peak. The large peak corresponds to non-resonant component caused by the steep pressure gradient region and the small peak to the resonant component, because the relation $p_1 \propto \frac{\phi_1}{x}\frac{d\beta_{eq}}{dx}$ is satisfied. The eigenfunctions ϕ_1 and ξ_r calculated at S=10^5 become more localized at the ι=1 surface in the cases of S=10^6 and 10^8.

For the $\beta_{eq}(x)$ profile with x_o=0.858 shown in Fig.8(a) aiming at simulating a radially expanded profile at the onset of an ELM, the growth rate (γ_1=1.482E-2) is enhanced by a factor of ~10 compared to the ELM free case with x_o=0.788 at S=10^5, as seen from Fig.6. Moreover, the eigenfunction ϕ_1 expands considerably inside the ι=1

surface. The ϕ_1 peak locates at x=0.924 and clearly deviates from the resonant surface, as seen from Fig.8(b). The reason why the peak of ϕ_1 deviates from the ι=1 surface is caused by overlapping the non-resonant part caused by the steep pressure gradient region on the resonant part. The eigenfunction ϕ_1 deviates noticeably from a pure interchange type which has a localized nature at the mode resonance surface having an even function. Nevertheless, the eigenmodes calculated here are the m=1/n=1 RIC modes. Of course, the linear code does not find any eigenmode solutions of the ELM because it should be excited as a result of the nonlinear evolution of linearly unstable RICs in LHD plasmas. The eigenfunction p_1 has a large single peak just inside the ι=1 surface, as shown in Fig.8(b). The eigenfunction of ξ_r also exhibits a similar character with ϕ_1, as shown in Fig.8(c). From the comparison of eigenfunctions shown in Figs. 7 and 8 together with Fig.6, the slight radial expansion which is inferred from the experimental data may trigger the large growth of the m=1/n=1 RIC, and accordingly induce a large amplitude ELM through nonlinear evolution of the RIC. These radially extended eigenfunctions may lead to a radially extended collapse of the ETB, as observed experimentally [8]. Strongly coupled RIC and ELMs play a critical role in the full destruction of the ETB or pedestal in the LHD H-mode, as seen from Figs. 1 and 4. It should be noted that the beta value $<\beta_{dia}>$ shown in Fig.1 increases at most about 25 % from the beginning to the end of each ELM free phase. If the pressure gradient would increase with the same increase rate in $<\beta_{dia}>$ without the radial expansion, the calculated growth rate γ_1 increases 1.6 times for the fixed x_o=0.788. It is not significant, compared with the increase in γ_1 in the order of magnitude with the radial expansion from x_o=0.788 to 0.858. Moreover, the width of the eigenfunction of ϕ_1 or ξ_r is about half of that calculated for the radially expanded case of x_o=0.858, so that the spatial impact of the mode on the ETB may not be significant as observed experimentally in the ELM. Although the radial expansion scenario seems to be likely compared with the above-mentioned increasing pressure gradient scenario based on the linear stability analysis, nonlinear simulations validated with the experimental results are needed to draw the definite conclusion.

On the other hand, in the L-phase the $\beta_{eq}(x)$ profile with x_o=0.560 has no steep pressure gradient, as shown in Fig.9(a). For the profile, the growth rate is γ_1=3.822E-3 and is by a factor of ~2.5 larger than that for the ELM-free H-phase profile with x_o=0.788. The eigenfunctions of ϕ_1, p_1 and ξ_r in the L-phase are shown in Figs.9(b) and (c). These eigenfunctions clearly localize at the ι=1 surface having an even function at the resonance surface, and indicates a typical RIC.

In all ψ_1 eigenfunctions shown in Figs.7(c), 8(c) and 9(c), ψ_1 does not vanish at

the ι=1 surface. This means that finite radial magnetic field $\underline{b_r}$ would be generated at the mode resonance surface, because $b_r = -\frac{im}{ax}\psi_1$. When the amplitude of the RIC grows nonlinearly to a certain level, the enhanced b_r would generate a magnetic island at the resonance surface. This process may play an important role in the ELM dynamics through such island formation.

5. Discussion

In Section 4, the dependence of the growth rates and eigenfunctions on the distance between x_o and x_s was analyzed. The linear MHD stability analysis suggests that if the pressure gradient at the resonance surface is maintained to be sufficiently low, edge stability against RICs will be improved even in the LHD configuration of which edge region is in the magnetic hill. The improved stability will bring about good plasma confinement of H-mode. A key factor of this favorable scenario is the ETB formation. That is, an ETB formation contributes to substantial reduction of heat and particle fluxes to the outside region where the main resonance surface ι=1 exists in the specific configuration of LHD, and prevents the increase of the pressure gradient at the ι=1 surface in the magnetic hill.

In actual experimental conditions, the distance $|x_o$-$x_s|$ will be more sensitively changed by the change of the ι=1 location x_s, because it is changed easily and appreciably by generation of even small co-flowing toroidal current and Shafranov shift. Co-flowing current of ~10 kA at B_t=0.9T is observed in the H-mode. It is roughly estimated that this current moves the resonance surface inward by Δx~0.03. This corresponds to the increase of x_o by ~0.03. On the other hand, the increase of the Shafranov shift due to the increase in $<\beta_{dia}>$ and the increase of the peaking factor of the pressure profile move the ι=1 surface outward through a decrease of the rotational transform in the edge region and an increase in the core region.

In Section 4, the dependences of the growth rates and eigenfunctions on the distance $|x_o$-$x_s|$ are studied using a linear resistive MHD code only including plasma resistivity [13]. The results provide insight into qualitative understanding of clear suppression and large growth of m=1/n=1 RIC observed in the H-mode in an outward-shifted configuration. Nevertheless, it is necessary to investigate whether or not diamagnetic effects may substantially change the dependence of growth rates and eigenfunctions on the distance $|x_s$-$x_o|$, because the diamagnetic drifts in H-mode become significant in the edge region. The relative position of the peak diamagnetic drifts to the ι=1 surface changes obviously by the scan of x_o discussed in Section 4. The

diamagnetic effects on the growth rates and eigenfunctions for the H-phase profiles in Section 4 are studied by using a newly developed eigenvalue code including resistivity and diamagnetic drifts [14]. For both profiles with x_o=0.788 and 0.858, the diamagnetic effects are fairly small, i.e., less than ~5 %, although the diamagnetic effects reduce the growth rate appreciably, i.e., up to 23 % in the profile with $x_o \sim 0.82$. In conclusion, the diamagnetic effects are weak even in the H-mode profiles corresponding to those in the ELM free phase (i.e., x_o=0.788) and at the onset of an ELM (x_o=0.858). A large non-resonant part inside the mode resonance surface in p_1 seen in Fig. 7(b) is appreciably suppressed by the diamagnetic effects, but the resonant part is appreciably enhanced. Detailed analyses are left for future study aiming at better understanding of RIC stability in the LHD H-mode plasmas.

The other interesting topic is to investigate the $|x_o-x_s|$ dependence of the growth rates in H-phase for further increased S that is expected in future high temperature H-mode plasmas on LHD. The x_o-dependence of the growth rates in H-phase is investigated for $S=10^8$ as shown in Fig.6. The growth rates in the range of x_o=0.788 to 0.858 follows the $S^{-1/3}$ dependence expected for RICs [15]. However, the peak growth rates around x_o~0.90-0.95 show much weaker S dependence than $S^{-1/3}$. At $S=10^8$, the growth rates increase more quickly toward the peak from the very low levels, as seen from Fig.6. This tendency is explained as follows. With the increase of S, the eigenfunction such as ϕ_1 becomes narrower and narrower. For the eigenfunction strongly localized at the mode resonance surface, the interaction of the eigenfunction with the steepest pressure gradient region will be suddenly enhanced when x_o is increased much closer to the location of the mode resonance surface at x_s=0.945. The peak growth rates at $S=10^8$ become insensitive with S in the range of x_o=0.90 to 0.93, indicating a character of ideal interchange mode. It will be necessary to control the steepest pressure gradient location more finely for the major mode resonance surface such as ι=1 for the suppression of large amplitude ELMs in high temperature H-modes with $S=10^8 \sim 10^9$ on future stellarator/helical devices.

6. Summary

In a specific magnetic configuration of LHD where the ι=1 surface is placed just outside the LCFS of the vacuum field, H-modes have been observed having long ELM free H-phases where RICs are clearly suppressed to an acceptable level for good plasma confinement. The H-mode character exhibits a clear contrast to that observed in the so-called inward-shifted configuration of LHD, where RICs are immediately enhanced by the ETB formation. Each long ELM free phase is interrupted by a large

amplitude ELM. The ELM is thought to be triggered by nonlinear growth of RIC and also enhances the RIC further through strong and complex coupling between RICs and ELMs. The H-L back transition is triggered by a large amplitude ELM. The numerical results obtained by two linear resistive MHD codes on the assumption of a cylindrical plasma have enabled a qualitative understanding of suppression and large growth of m=1/n=1 resistive interchange modes observed in the H-modes in the outward-shifted configuration. Nonlinear simulations of the RIC modes in the realistic LHD configuration are of great importance for better understanding of the nonlinear growth of RIC, ELM trigger and the strong coupling between RICs and ELMs in stellator/helical plasmas.

Acknowledgements

We acknowledge the LHD technical team for their excellent support in this research. This research is supported in part by LHD project budgets (NIFS10ULHH011, NIFS14KLPP037 and NIFS12KLPP025) and the Grant-in-Aid for Scientific Research from JSPS (No. 24360386, No. 26630476). It is also supported by the JSPS-NRF-NSFC A3 Foresight Program in the field of Plasma Physics (NSFC: No.11261140328, NRF: No. 2012K2A2A6000443).

References

[1] A. Loarte et al., Chapter 4 in *the Progress in the ITER Physics Basis*, Nucl. Fusion **47** (2007) S203.
[2] A. Loarte et al., Plasma Phys. Control. Fusion **45** (2003) 1549.
[3] P.B. Snyder et al., Phys. Plasmas **9** (2002) 2037.
[4] G.T.A. Huijsmans et al., Phys. Plasmas **22** (2015) 021805.
[5] A. Weller et al., Phys. Plasmas **8** (2001) 931.
[6] K. Toi et al., Phys. Plasmas **12 (**2005) 020701.
[7] K. Toi et al., Fusion Sci. Technol. **58** (2010) 61.
[8] K. Toi et al., Nucl. Fusion **54** (2014) 033001.
[9] F. Watanabe et al., Contrib. Plasma Phys. **50** (2010) 651.
[10] Y. Suzuki et al., Nucl. Fusion **46** (2006) L19.
[11] K. Ogawa et al., Plasma Fusion Res. **3** (2008) 030.
[12] Y. Takemura et al., Plasma Fusion Res. **8** (2013)1402123.
[13] R. Ueda et al., Phys. Plasmas **21**, 052502 (2014).
[14] T. Nicolas and K. Ichiguchi, Nucl. Fusion **56** (2016) 026008.
[15] B.A. Carreras et al., Phys. Fluids **30** (1987) 1388.

Figure Captions

Fig.1 (a) Typical waveforms of an H-mode with long ELM free phases and large amplitude ELMs in the outward-shifted magnetic configuration of R_{ax}=3.9m, where W_p, $<n_e>$ and H_α are the plasma stored energy measured by a diamagnetic loop, line averaged electron density and H_α emission, respectively. (b) Time evolution of the root-mean-square amplitude of magnetic fluctuations associated with the m=1/n=1 mode together with the volume-averaged toroidal beta $<\beta_{dia}>$ evaluated from W_p.

Fig.2 Radial profiles of electron temperature (T_e), electron density (n_e) and electron pressure (P_e) obtained from the Thomson scattering in the characteristic phases, "H" and "L" in the H-mode plasma, which are shown as a function of major radius R in the horizontally elongated section. The vertical arrows indicate the inferred location of the ι=1 mode resonance surface.

Fig.3 The radial profiles of the H_α emission intensity (open triangles) and the coherence between H_α and magnetic fluctuations induced by the m=1/n=1 mode (open circles), as a function of the normalized vertical coordinate Z/Z_a, where Z_a is the plasma boundary in the vertical direction. The vertical line indicates the expected location of the ι=1 surface.

Fig.4 (a) and (b) Zoomed waveforms of two typical large ELMs in the H-mode shot shown in Fig.1, where the signal of poloidal magnetic field fluctuations (b_θ), H_α emission signal and line electron density just outside the ETB boundary (n_eL_{edge}) are shown. The vertical line indicates the onset time of the small crash in n_eL_{edge} as a signature of an ELM.

Fig.5 (a) Experimental data points of the total bulk plasma pressure $P_{eq}(x)$ in the H-phase (t=4.533 s) and the best-fitted curve with eq.(1). (b) Experimental data points of $P_{eq}(x)$ in the L-phase (t=4.700s) and the best-fitted curve. For the radial coordinate $x=<r>/a$ with a=0.466 m, the ι=1 surface location is inferred to be

x=1.05-1.08.

Fig.6 Dependence of the largest normalized growth rates of the m=1/n=1 RICs on the location of the steepest pressure gradient x_o in the H- and L-phase profiles for S=10^5 and 10^6. The growth rates in the H-phase are also given for S=10^8. The growth rates are shown in linear and log-scales in (a) and (b), respectively. Two arrows on H-phase profiles indicate the profiles in the ELM free phase (x_o=0.788) and at an onset of an ELM (x_o=0.858). The arrow on the L-phase profiles indicates the profile observed experimentally.

Fig.7 (a) $P_{eq}(x)$ profile with x_o=0.788 to simulate an ELM free H-phase and the rotational transform profile $\iota(x)$. (b) m=1/n=1 eigenfunctions of the scalar potential ϕ_1 and pressure perturbation p_1. (c) Eigenfunctions of poloidal flux ψ_1 and radial displacement ξ_r, where S=10^5. The vertical line in all three figures indicates the location of the ι=1 surface, and also in Figs.8 and 9.

Fig.8 The m=1/n=1 eigenfunctions of ϕ_1 and p_1 (b), and ψ_1 and ξ_r (c), calculated for the $P_{eq}(x)$ profile with x_o=0.858 to simulate the onset phase of a large ELM (a), where S=10^5.

Fig.9 The m=1/n=1 eigenfunctions of ϕ_1 and p_1 (b), and ψ_1 and ξ_r (c), calculated for the $P_{eq}(x)$ profile with x_o=0.560 to simulate the L-phase, where S=10^5.

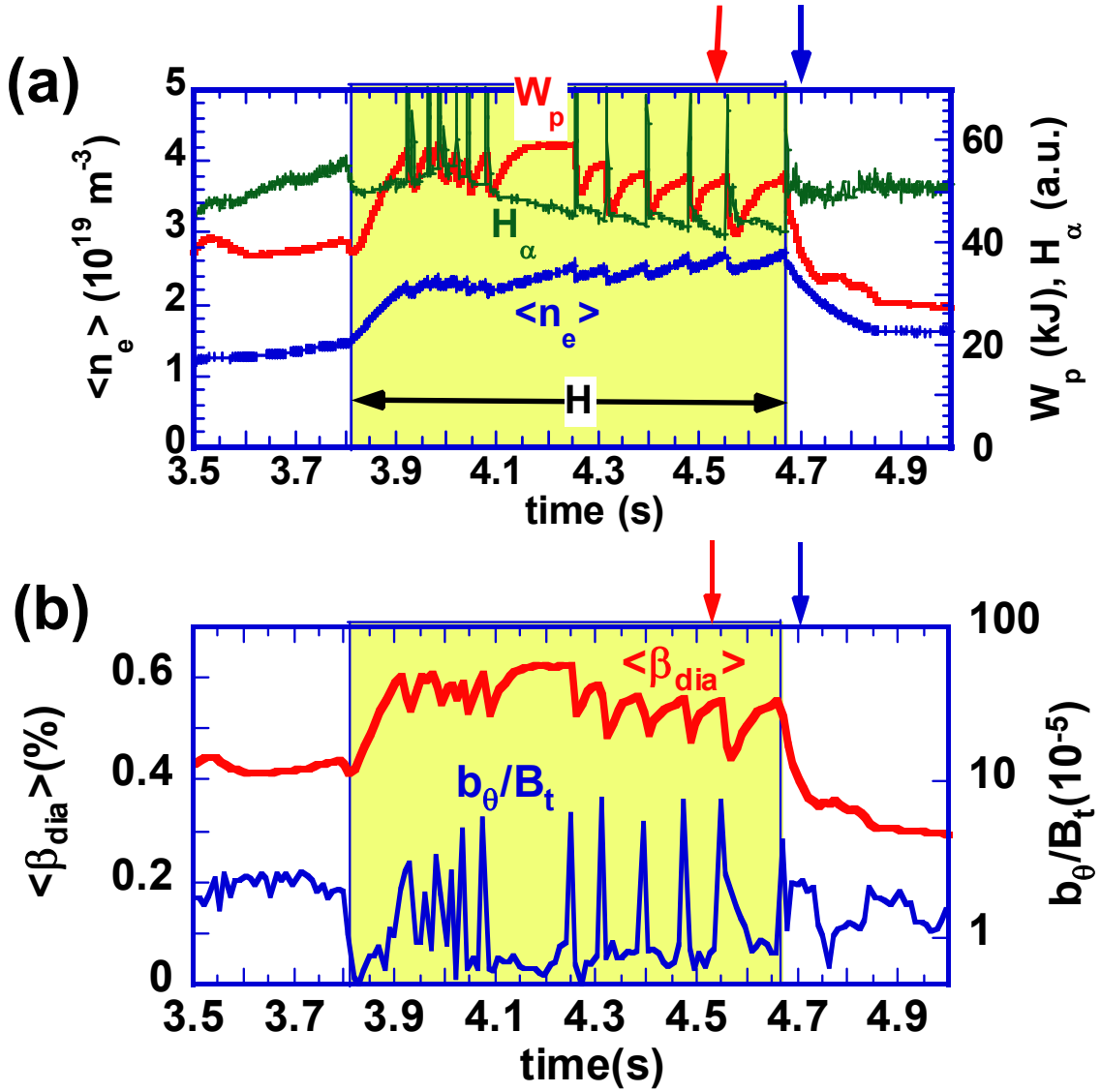

Fig.1 K. Toi et al.

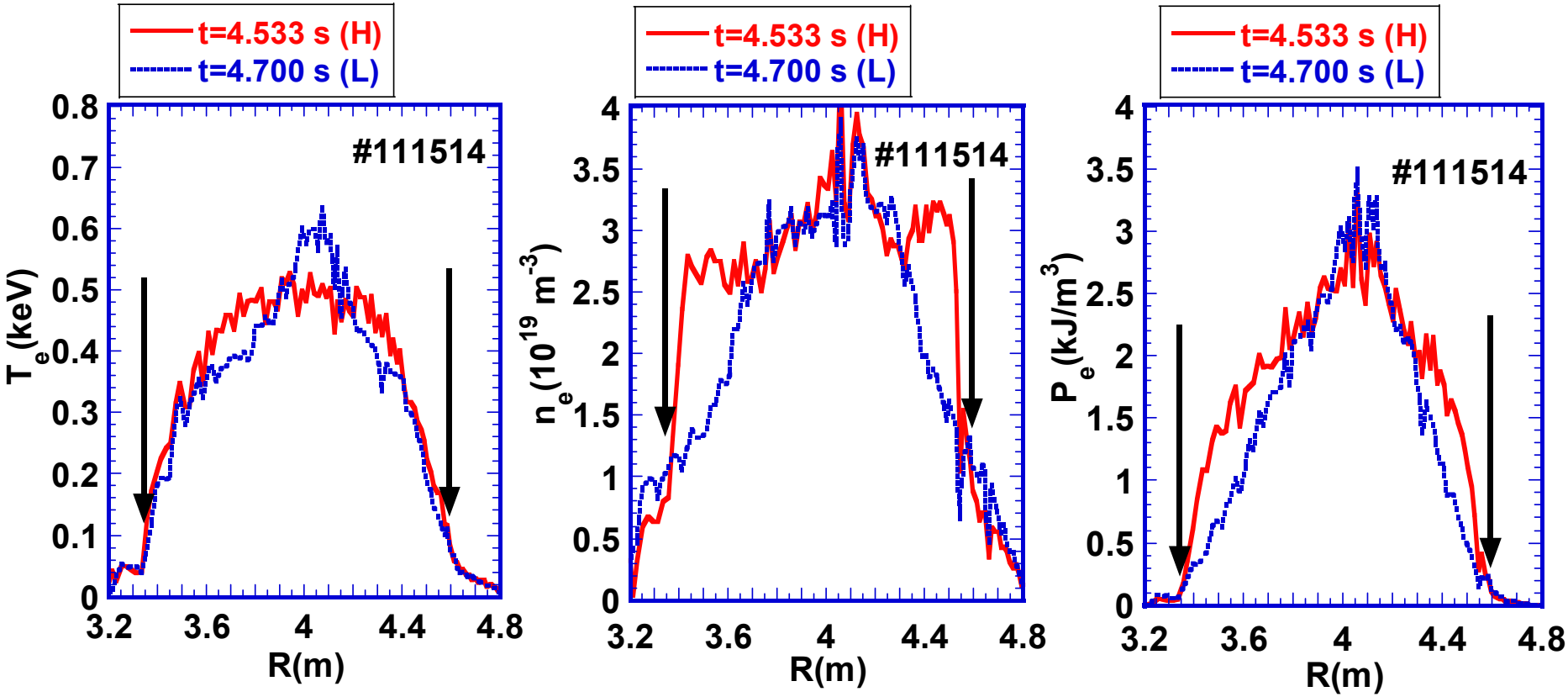

Fig.2 K. Toi et al

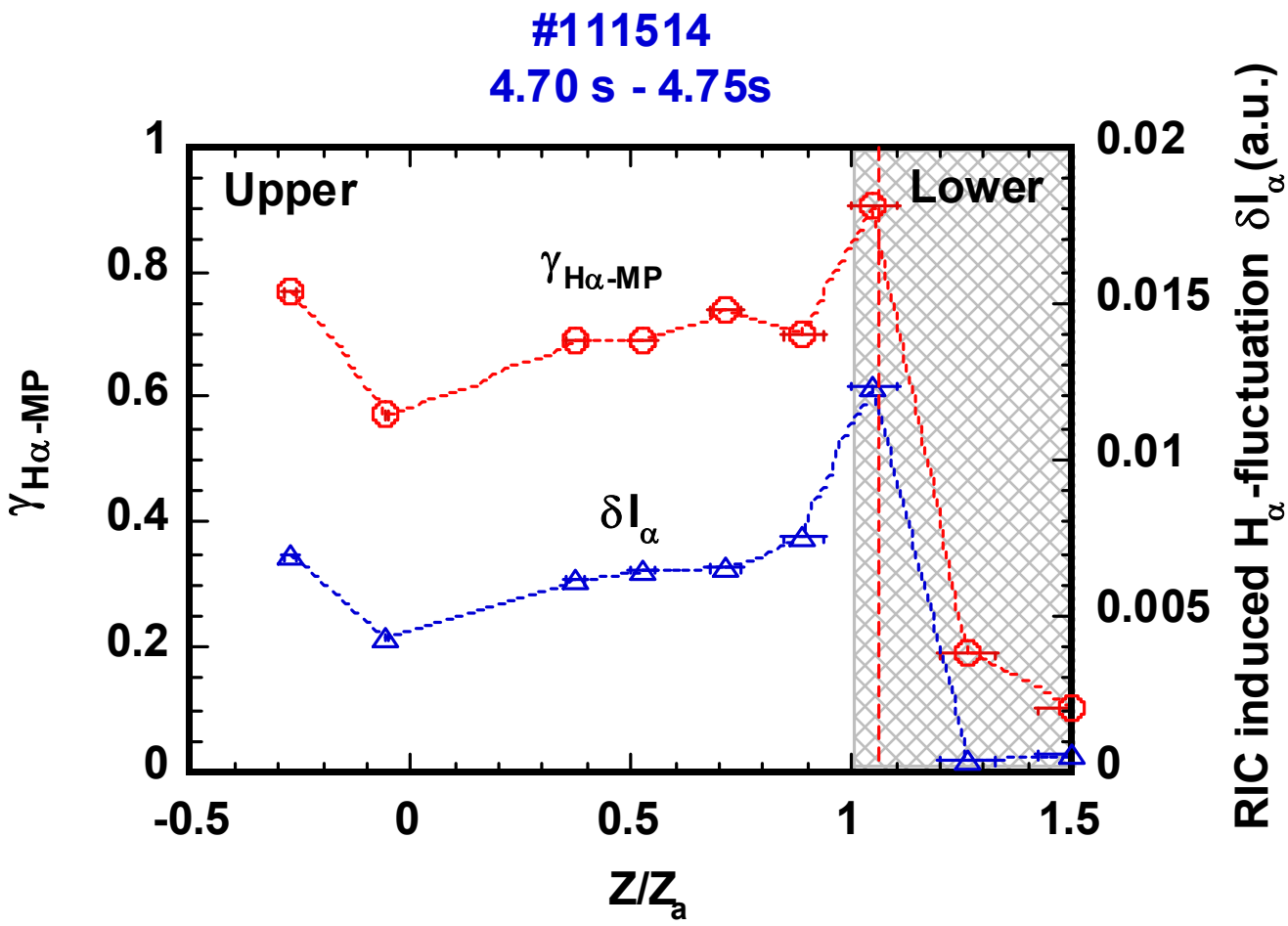

Fig.3 K. Toi et al.

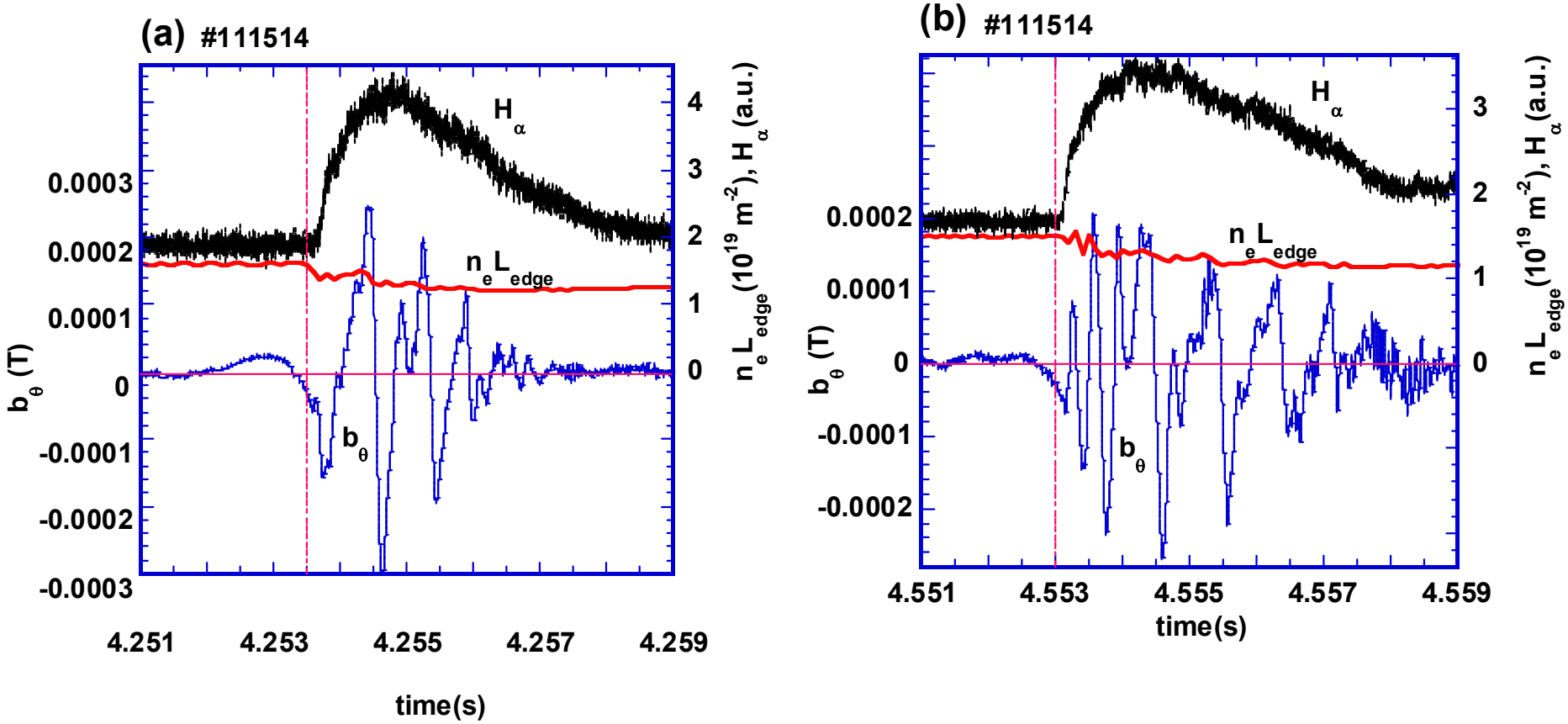

Fig.4 K. Toi et al.

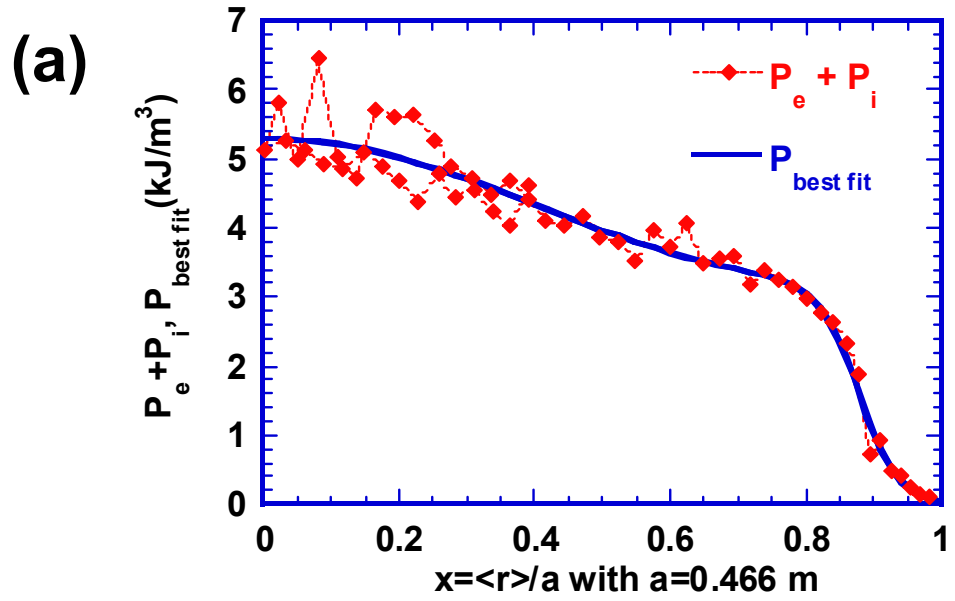

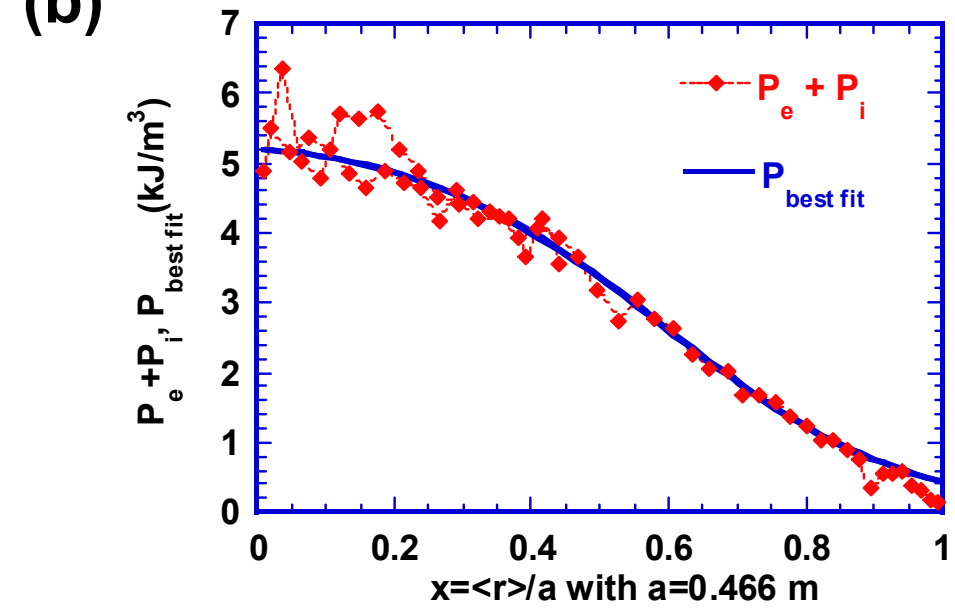

Fig.5 K. Toi et al.

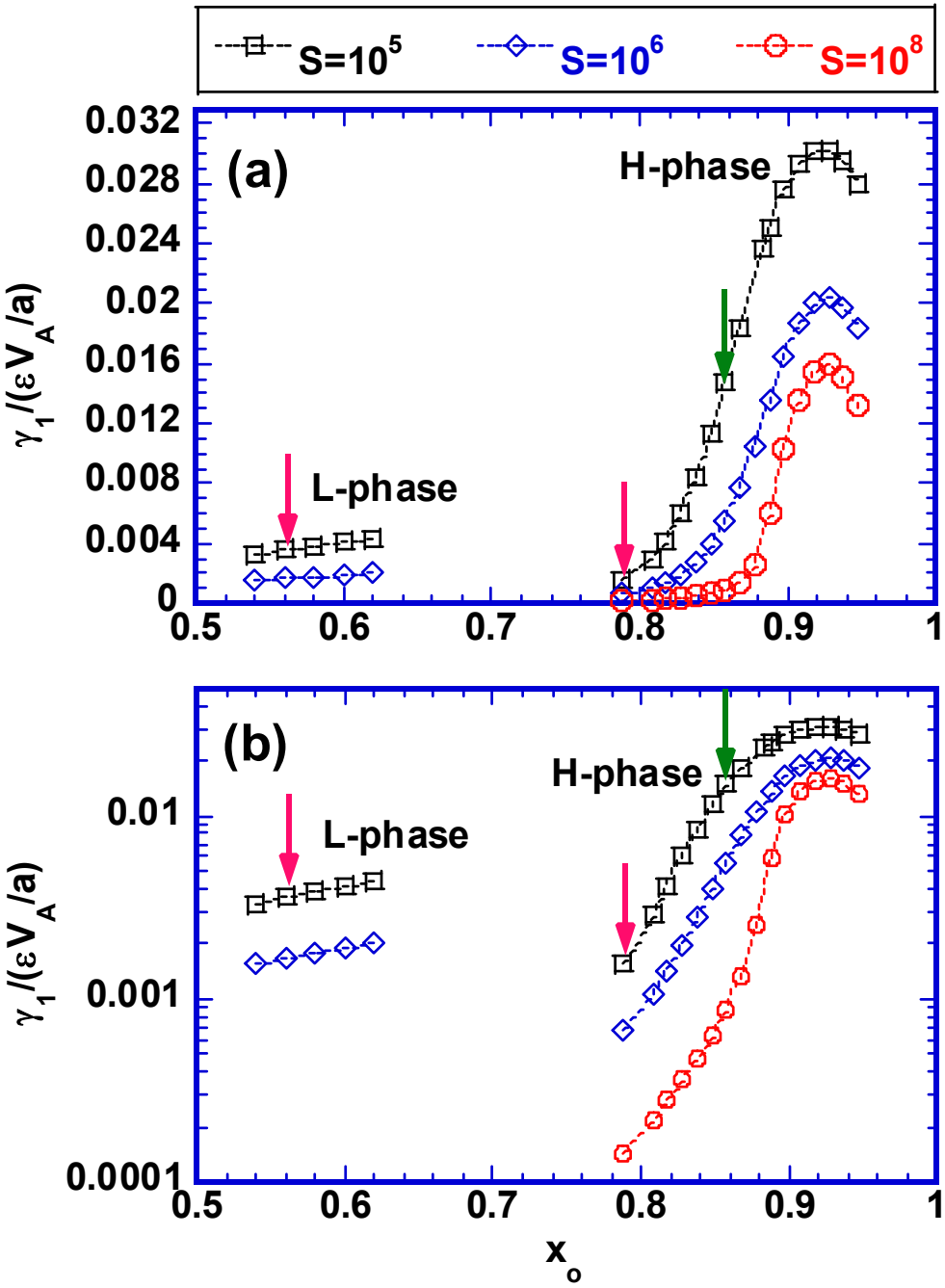

Fig.6 K. Toi et al.

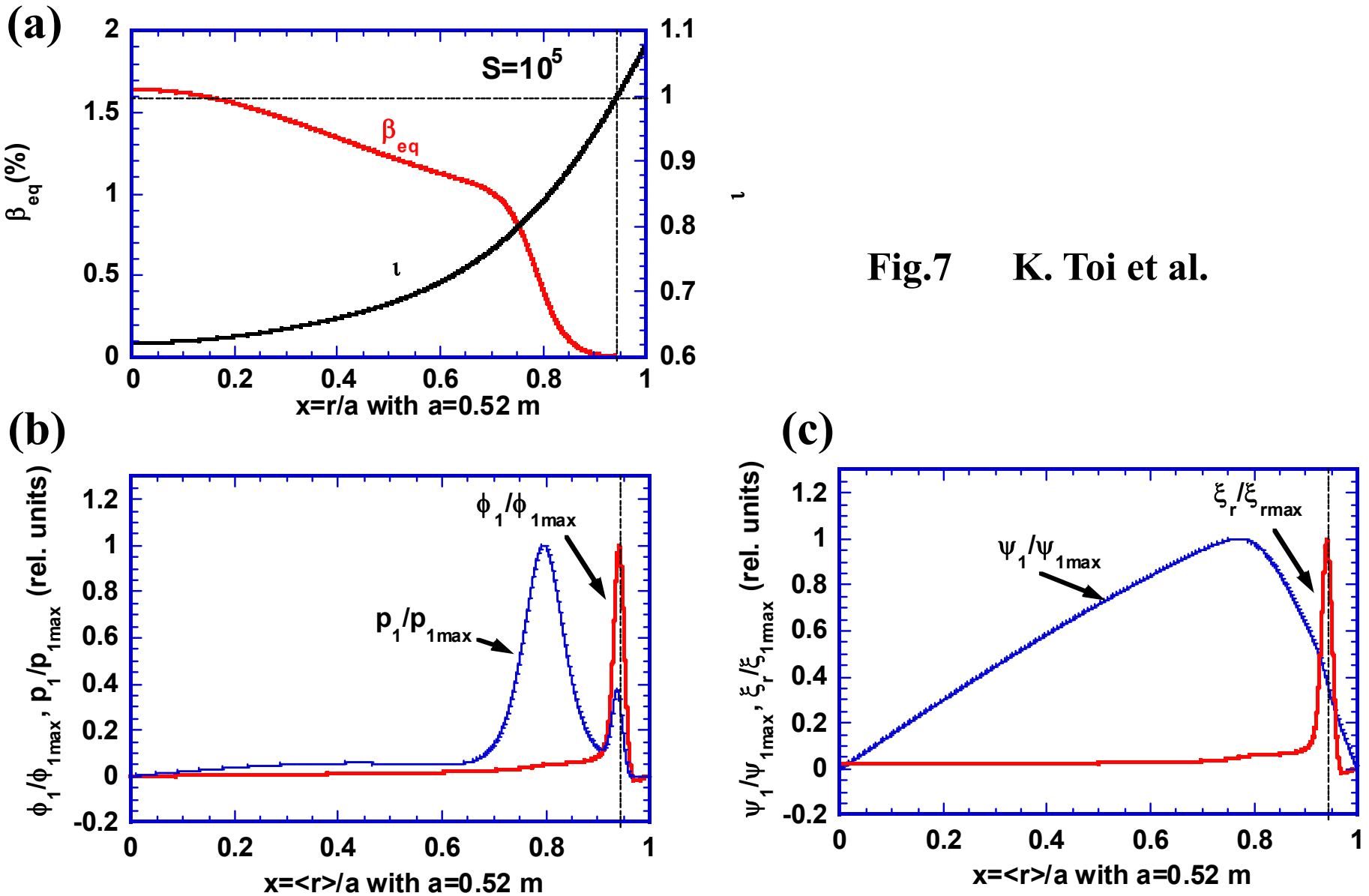

Fig.7 K. Toi et al.

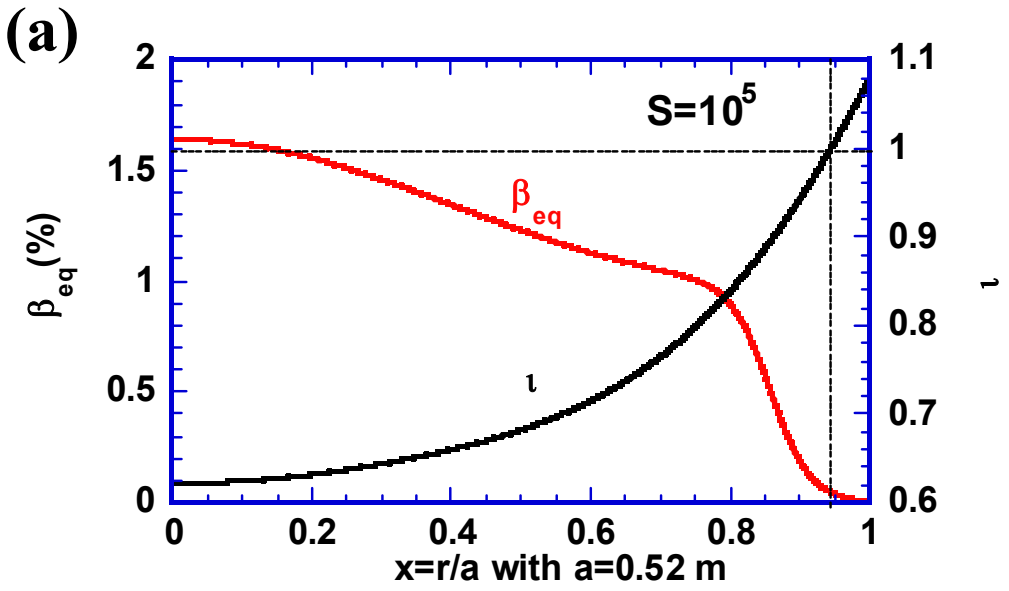

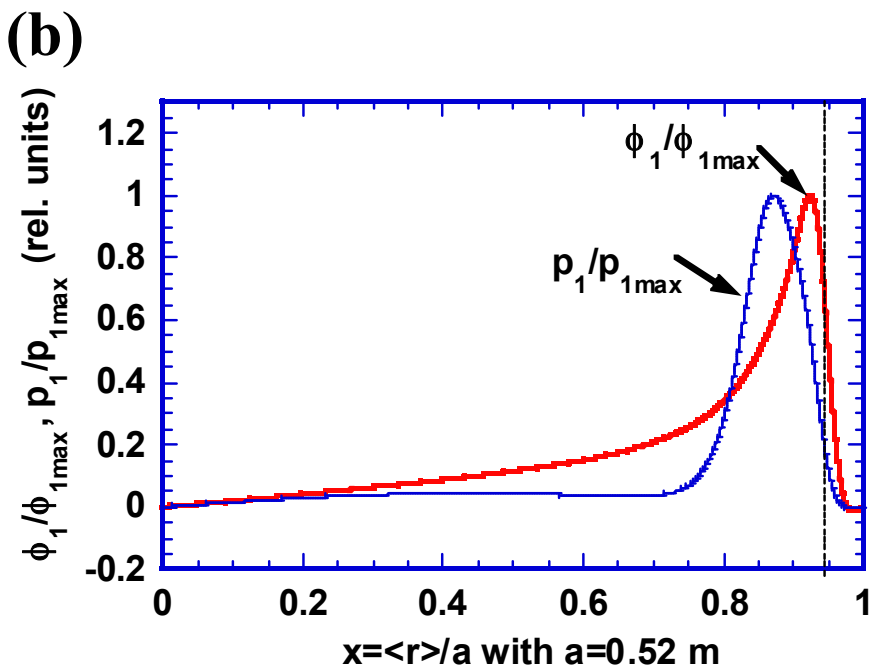

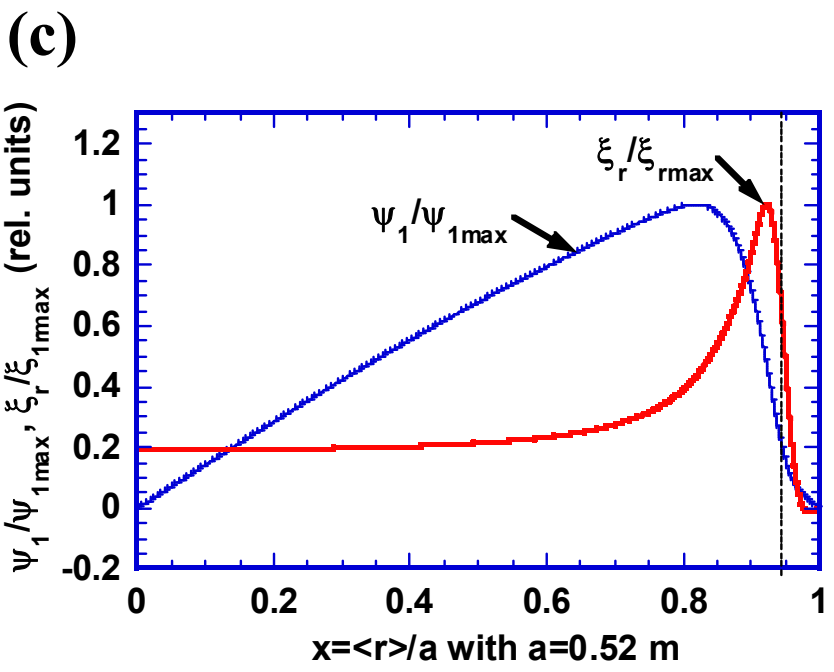

Fig. 8 K. Toi et al.

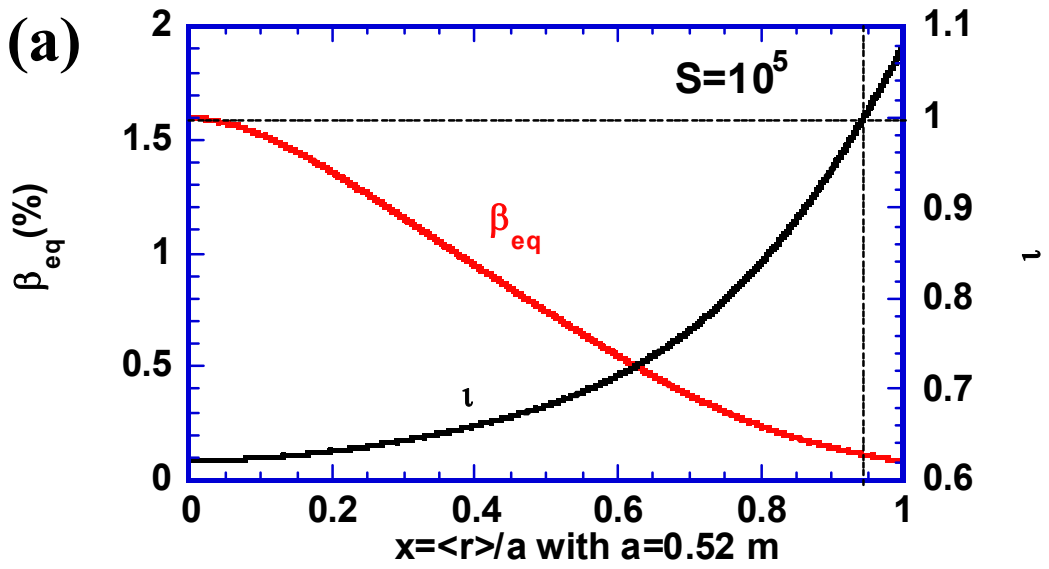

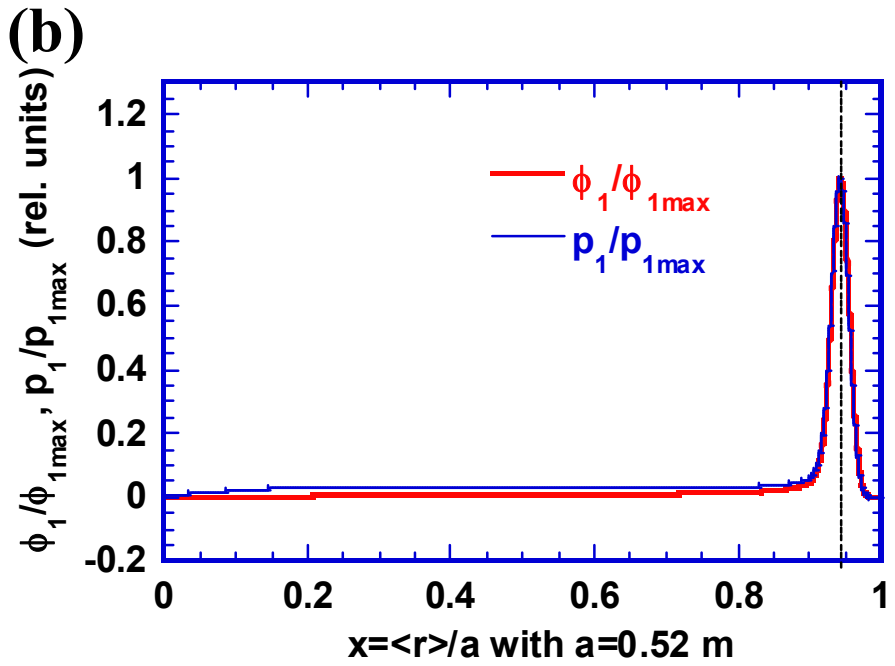

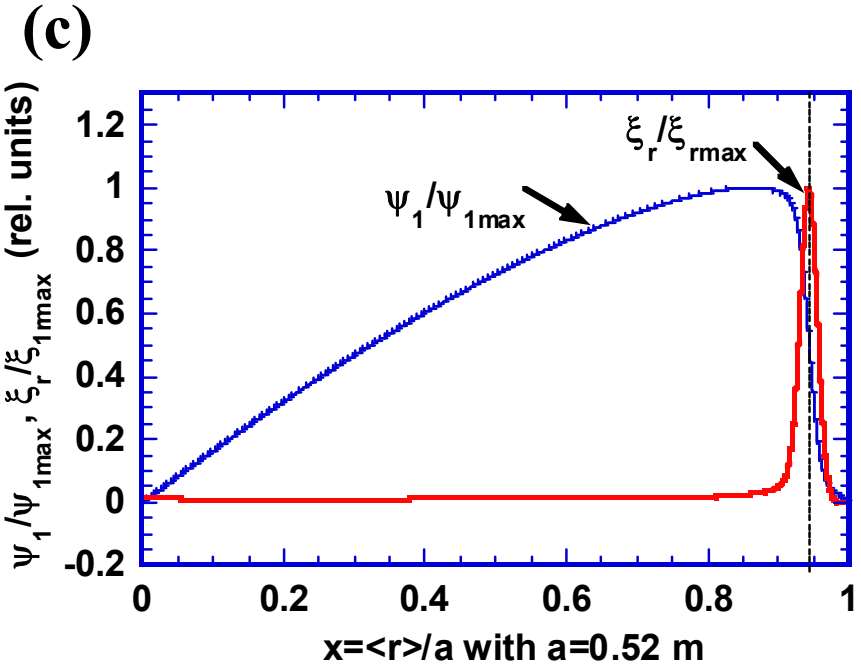

Fig.9 K. Toi et al.